

Why Are Carbon Nanotubes Fast Transporters of Water?

Sony Joseph and N. R. Aluru*

Department of Mechanical Science and Engineering, Beckman Institute for Advanced Science and Technology, University of Illinois at Urbana-Champaign, Urbana, Illinois 61801

Received September 17, 2007; Revised Manuscript Received December 11, 2007

ABSTRACT

Extraordinarily fast transport of water in carbon nanotubes (CNTs) in recent experiments has been generally attributed to the smoothness of the CNT surface. Using molecular dynamics simulations we investigate water flow in (16,16) CNTs and show that the enhanced flow rates over Hagen–Poiseuille flow arise from a velocity “jump” in a depletion region at the water nanotube interface and that the water orientations and hydrogen bonding at the interface significantly affect the flow rates. For nanotube with the same smooth wall structure but with more hydrophilic Lennard-Jones (LJ) parameters of silicon, the enhancement is greatly reduced because it does not have “free” OH bonds pointing to the wall as in CNTs that would reduce the number of hydrogen bonds in the depletion layer. Roughness in the tube walls causes strong hydrogen-bonding network and no significant flow enhancement is attained in rough tubes.

Dramatic enhancement of pressure driven flows of water through carbon nanotubes as compared to other porous materials has gained considerable attention recently due to its potential applications in drug delivery, biomimetic selective transport of ions, etc. Pressure driven flow velocities of 4 or 5 orders of magnitude higher than predicted from Newtonian Flow using the Hagen–Poiseuille equation has been observed in multiwalled carbon nanotube (MWNT) membrane pores of 7 nm inner diameter by Majumder et al.¹ More recently, in double walled carbon nanotube (DWNT) pores with an inner diameter of 1.6 nm the measured water flow exceeds values calculated from continuum hydrodynamics models by more than 3 orders of magnitude.² Molecular dynamics (MD) studies of gases with exceptionally high transport rates of methane and hydrogen in nanotubes are shown to be a result of the inherent smoothness of the nanotubes³ and low friction at the surface.⁴ A review of recent literature and a detailed discussion of flow in nanotubes can be found in ref 5. Although water structure in nanotubes has been studied extensively using MD simulations,^{6–12} the emphasis has been mainly devoted to small diameter tubes in which bulk properties of water have not been attained at the tube center. For narrow (6,6) tubes, large flow rates in carbon nanotubes have been attributed to the single file water structure and the associated hydrogen bonding.¹⁰ In narrow (8,8) tubes, long-lasting hydrogen bonds are responsible for the fast diffusion of water clusters.¹³ Though many MD studies have dealt with diffu-

sion and filling mechanism of water in carbon nanotubes, relatively fewer studies have investigated velocity profiles under an external driving force.^{14,15}

Recent experiments have conclusively shown that water, on meeting a hydrophobic solid, forms a thermodynamically driven low-density depletion layer.¹⁶ In carbon nanotubes, water structure in the interfacial depletion region and its relation to the flow is not well understood. In this paper, using MD simulations we relate the water structure in the depletion layer such as water orientations and the hydrogen bonding to the velocity “jumps” observed in the flow. The main factors that influence the velocity “jumps” at the interface are the local intermolecular interactions and the surface roughness.¹⁷ To investigate the effect of these factors on the flow rates, we chose three smooth tubes with water accessible diameter of approximately 1.6 nm, the same as that used in experimental studies² but with different Lennard-Jones (LJ) parameters and one tube with the same LJ parameters and inner diameter as that of carbon nanotube (CNT) but with wall roughness.

For the MD simulations, the different types of tubes considered were (i) (16,16) CNT with a bond length of 0.142 nm, modeled as LJ atoms because the partial charges for CNTs are significant only for finite tubes,¹⁸ (ii) (16,16) boron nitride nanotube (BNNT) with a bond length of 0.144 nm, (iii) (16,16) nanotube with the same smooth structure as CNT but with much more attractive LJ parameters of silicon, and (iv) a rough tube whose six-ring unit cell comprises of a three-ring (16,16) CNT and a three-ring (18,18) CNT. The center to center distance for the (16,16) nanotube is

* Corresponding author. E-mail: aluru@uiuc.edu. URL: <http://www.uiuc.edu/~aluru>.

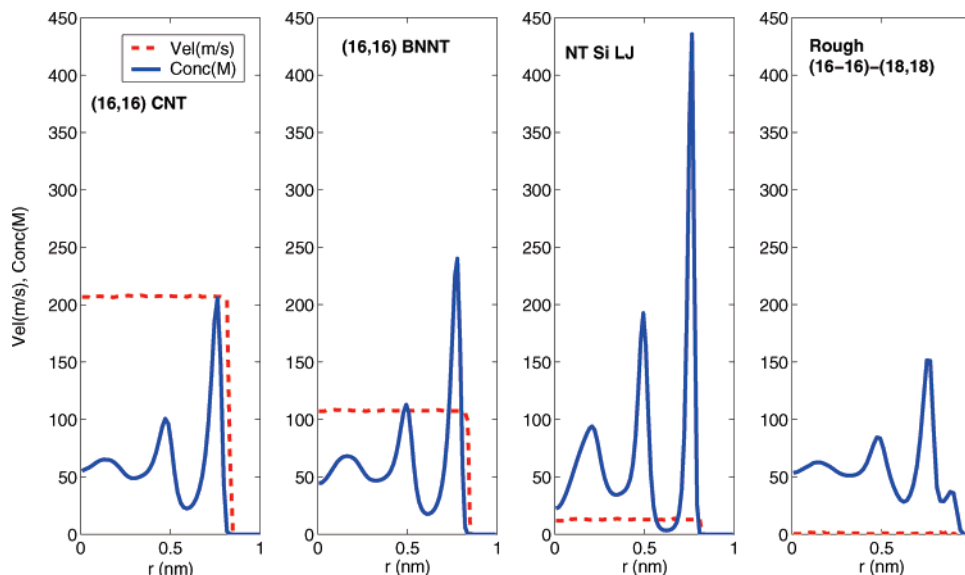


Figure 1. Water concentration and axial velocity profiles as a function of the radial distance toward the wall from the center of the tube at $r = 0$ nm. Only one-half of each tube cross-section is shown. From the left to the right are (i) (16,16) CNT, (ii) (16,16) BNNT, (iii) (16,16) NT with Si LJ, and (iv) rough tube with alternating sections of (16,16) and (18,18) tubes. For the first three cases, even though the tubes have smooth surfaces, the magnitude of the flow velocities show marked differences. The bulk concentration is 55 M.

2.17 nm and for the (18,18) tube is 2.44 nm. The LJ parameters for carbon were taken from ref 18, boron and nitrogen were taken from ref 19, and that for silicon was taken from ref 20. It should be noted that the walls of a silicon nanotube cannot have a planar sp^2 structure like a CNT, but to distinguish between the effects caused by smoothness and an attractive LJ interaction we use an artificial tube with the same geometry as a CNT but with LJ parameters of silicon. MD simulations were performed with Gromacs 3.3.1,²⁰ using a time step of 2 fs. The flow was simulated in infinitely long tubes with periodic boundary conditions and box lengths of 7.87, 7.98, 7.87, and 8.21 nm, respectively, in the axial direction. For gases, only in the limit of low density at a pressure less than 1 bar does the tube flexibility reduce the diffusion of methane in CNTs such that rapid transport is not attained.^{21,22} Simulations of nonequilibrium flow of water in CNTs have used rigid tubes in the past.^{14,15} For water, our preliminary simulations showed that extraordinary enhancements are present with or without flexible walls with flexibility increasing the mean velocity by 10–20%. For the sake of simplicity, we used a rigid fixed tube. Water was modeled by using the SPC/E model.²³ The temperature of the fluid was maintained at 300 K by using a Nose–Hoover thermostat^{24,25} with a time constant of 0.2 ps. For calculating the temperature, the mean axial velocity of water was subtracted from the axial component of the velocity of each water molecule as implemented in ref 20. The long-range electrostatic interactions were computed by using a particle mesh ewald method²⁰ (real space cutoff, 1.0 nm; FFT grid spacing, 0.12 nm, fourth-order interpolation). The short-range interactions were computed using a cutoff scheme (cutoff distance, 1.0 nm). Starting from a configuration of a randomly solvated system with fixed slabs of size $3.2 \times 3.2 \text{ nm}^2$ and baths of $3.2 \times 3.2 \times 1.5 \text{ nm}^3$ attached at both the ends of the CNT, each system was simulated for 1.0 ns by maintaining a pressure normal to the slab with a

Parrinello–Rahman barostat²⁶ of 1 bar (compressibility time constant of 0.2 ps; compressibility of $4.5 \times 10^{-5} \text{ bar}^{-1}$). The water concentration at the ends of the bath was verified to be within 1% of the bulk water concentration of 55 M after 1 ns of simulation. Then the baths were removed and a production run of 10 ns was performed at constant volume to gather the statistics of various quantities, for example, the fluid velocity. A constant external acceleration, a_{ext} , applied along the channel in the Z-direction was used to drive the flow. A strong external acceleration ($a_{\text{ext}} = 0.002 \text{ nm/ps}^2$) was used in our simulations so that fluid velocity profile could be retrieved with reasonable accuracy with minimal fluctuations in the velocity profile due to thermal noise. The driving force on each molecule is less than 18% of $0.1 (\epsilon/\sigma)$, the driving force widely used in nanoporous simulations²⁷ and is equivalent to an effective pressure of 13.86 MPa (assuming a bulk density of 990 kg/m^3). The statistics were gathered after steady-state velocities are reached within 1–2 ns. To derive accurate velocity profiles, the velocities and concentration profiles were sampled at intervals of 2 fs.

Figure 1 shows the water concentration and velocity distribution across the various tubes considered. The concentrations and velocities are computed by averaging over the axial length of the tube for all time frames after steady-state velocity profiles have been reached. Apart from the well-known layering of water near the channel wall, we also observe that (1) there is a large velocity with a pluglike flow profile with a velocity “jump” at the interfacial region for all nanotubes except for the rough surface, (2) the magnitude of the velocity “jump” decreases with increasing concentration of the first water layer for smooth surfaces. The velocity profiles for the CNT, BNNT, and NT with Si LJ are similar to the pluglike flow profiles observed in flow under external forces.^{14,15} From the concentration and velocity profiles, a net mass flow rate can be computed and compared with that from continuum theory. The mass flow rate in a pipe

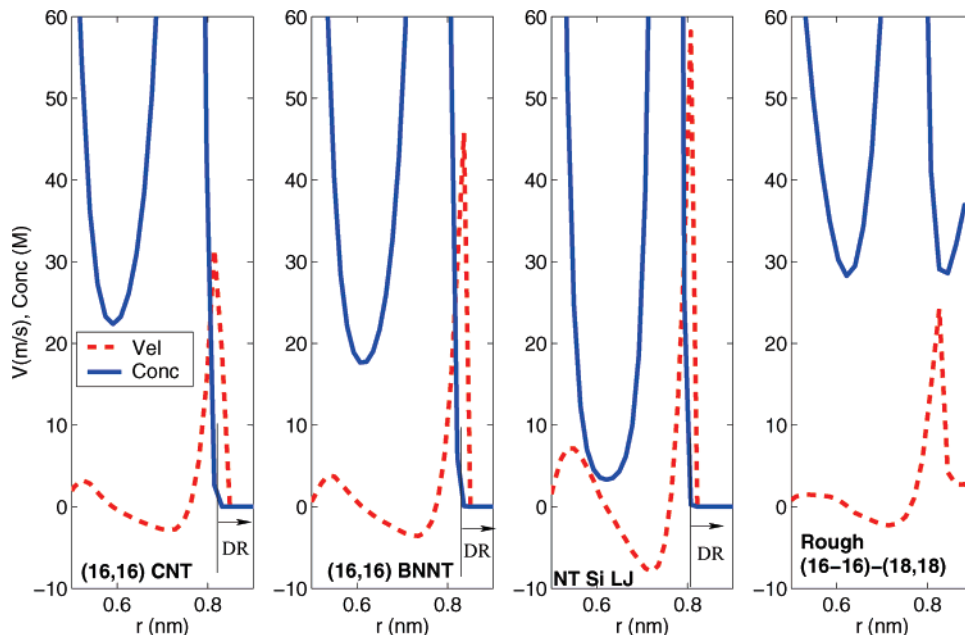


Figure 2. Water concentration and radial velocity profiles as a function of the radial distance from the tube center. The radial velocity is defined positive in the direction from the center toward the wall. Shown from the left to the right, are: (i) (16,16) CNT, (ii) (16,16) BNNT, (iii) (16,16) NT with Si LJ, and (iv) rough tube with alternating sections of (16,16) and (18,18) tubes. The radial velocity in the depletion region increases with increasing water concentration in the first water peak. The depletion region is denoted as DR.

according to continuum theory is $\dot{m} = \pi r^4 \rho^2 a_{\text{ext}} / 8\mu$, where r is the radius of the tube, ρ is the density, and μ is the dynamic viscosity. Using bulk values at 300 K for ρ and μ and an inner diameter computed by subtracting twice the Lennard-Jones σ from the center-to-center diameter, the enhancement of mass flow rates over that of continuum theory is 2052, 1142, 155, and 4.7 for CNT, BNNT, NT with Si LJ, and the rough tube, respectively. The enhancement in CNTs is within the range of the enhancement from 560 to 8400 observed in experiments for tubes of inner diameter of 1.6 nm.² In Figure 2, the radial velocity profiles are plotted along with the concentration profiles. Radial velocity is positive in the direction from the center to the wall. According to the continuum theory, for pipe flow the radial velocity components are zero. Here, we find a considerably large radial velocity in the tube that is related to the layering of the concentrations. A quasi-steady-state concentration gradient can give rise to a steady-state flow. As the peaks of the concentration profiles increase in magnitude from CNT to NT with Si LJ, the magnitude of the radial velocity also increases. In the interfacial region between the first peak and the wall, the radial velocity is the largest.

In recent years, questions have been raised whether there are nanobubbles or depletion layers at the interface of liquids near hydrophobic surfaces where velocity “jumps” occur. Recent X-ray reflectivity measurements of the interface between water and smooth hydrophobic monolayers conclusively show a depletion layer with a substantially lower density than the bulk water density with a thickness of one water molecule that cannot be explained by nanobubbles.¹⁶ It is important to note that the location of the velocity “jump” in our simulations is in a depletion region where the concentration is less than 5% (2.8 M) of the bulk water concentration of 55 M. The depletion regions in X-ray

measurements are based on one-dimensional (1D) electron density profiles as a function of the wall normal distance, which averages out the effects of the topography of the wall structure. To understand how the water structure in the depletion layer correlates to the underlying wall structure, 2D contours of the concentration profiles for oxygen atoms and hydrogen atoms in water in the depletion region are shown for CNT (Figure 3, top row) and NT with Si LJ (Figure 3, bottom row). The 2D profiles are plotted in cylindrical polar coordinates as a function of the axial distance z and circumferential angle θ with concentrations averaged over time for the entire length of the simulation after reaching steady-state for a thickness $\Delta r = 0.028$ nm at the location of the velocity “jump” at $r = 0.821$ nm for CNT and $r = 0.807$ nm for NT with Si LJ. Also shown are the projection of the hexagonal arrangement of the wall atoms beneath the water layer. For CNT, even though the concentration is quite low compared to the bulk there is some concentration of oxygen atoms above the centers of the hexagonal rings of the carbon atoms, and the rest of the interface is depleted (Figure 3, top left). The hydrogens are spread throughout the surface but with no clearly distinguishable pattern (Figure 3, top right). On the other hand, for the NT with Si LJ, even though the locations just above the wall atoms are depleted of oxygens, there is a clear difference in concentrations in the center of the hexagonal rings compared to the rest of the surface with the concentrations at the center of the rings being as high as 40 M (Figure 3, bottom left). With hydrogens too, a clear pattern emerges where the hydrogen atoms prefer to be in regions away from the centers of the hexagonal rings. For the NT with Si LJ, the water structure is such that the water forms a well-defined layer to correspond to the underlying hexagonal pattern of the wall atoms such that the oxygen atoms are in the center of the

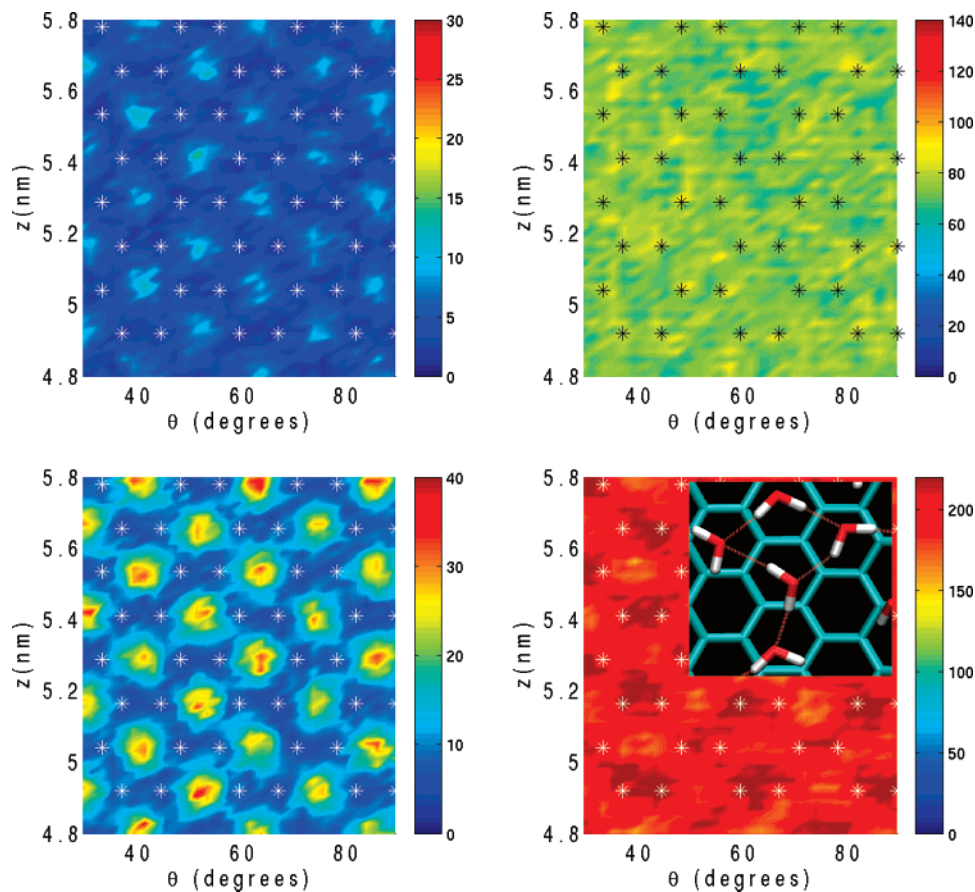


Figure 3. Time averaged 2D concentration contours of oxygens (top left) and hydrogens (top right) near the surface of a (16,16) CNT. The θ - and z -axes denote circumferential and axial variations, respectively. The color scale on the right of each plot represents the molar concentration. The * symbol denotes the position of the underlying wall atoms. Also shown are the contours of oxygens (bottom left) and hydrogens (bottom right) near the surface of a (16,16) nanotube with LJ parameters of Si. The snapshot of the depletion region in the bottom right figure shows the oxygens predominantly congregating at the center of the hexagonal rings to form a hydrogen-bonded water layer in the circumferential plane.

hexagonal ring where the wall Lennard-Jones interactions are attractive, rather than in the repulsive region above the wall atom. This is depicted in a snapshot shown in the inset of Figure 3 (bottom right). Although not shown here, the 2D water structure in the depletion region of BNNTs shows characteristics intermediate to that of CNT and NT with Si LJ. For the rough CNT, the 1D concentration profile does not show any depletion region (Figure 1) with the lowest average water concentrations being 30 M in the region $r = 0.821$ nm. This is consistent with the conclusions that there are no depletion regions for rough hydrophobic surfaces.¹⁶

To further understand the water structure in the depletion region, we investigate the water dipole and OH bond orientations in the depletion region. The top rows in Figure 4 shows the distribution of the average water dipole orientation with respect to the radial direction (0° is normal to the wall, pointing toward the wall) at different radial locations for the different wall structures considered. The bottom rows of Figure 4 depict the distributions of OH bond vectors. The distributions are normalized so that the bulk value is 1. The radial locations represent (i) the depletion region ($r = 0.807$ nm or $r = 0.821$ nm depending on the wall structure), (ii) the region of the first water peak ($r = 0.764$ nm or $r = 0.779$ nm), and (iii) the region of the valley

of the first water peak ($r = 0.636$ nm). For the rough tube, an additional radial location in the cavity formed by the roughness at $r = 0.879$ is also considered. A schematic of the water orientations inferred from the orientational distributions is shown in Figure 5. For the CNT, in the depletion region the dipoles mainly lie in the region $55^\circ < \theta < 80^\circ$. The OH bonds show peaks in the region $0^\circ < \theta < 15^\circ$ and $95^\circ < \theta < 120^\circ$. This corresponds to the water molecule in the depletion region with one OH bond pointing toward the wall and the other pointing toward the waters in the peak region. The water orientation in the depletion region is very similar to the experimental measurements of orientational distribution of water near hydrophobic surfaces that show “free” OH bonds or “dangling bonds” at the interface that protrudes into the organic molecules.^{28,29} In the region of the first water peak, both the OH bond vectors and the dipoles are mainly oriented at 90° to the radial direction such that the water forms a planar structure that could induce hydrogen bonding with each other. In the valley of the first peak, the water orientation is such that one OH vector points toward the center of the tube with an OH bond angle of 160 – 180° and the other at an angle of 60 – 80° . For the NT with Si LJ, unlike the CNT the orientations in the depletion region and the first water peak are similar with majority of the waters

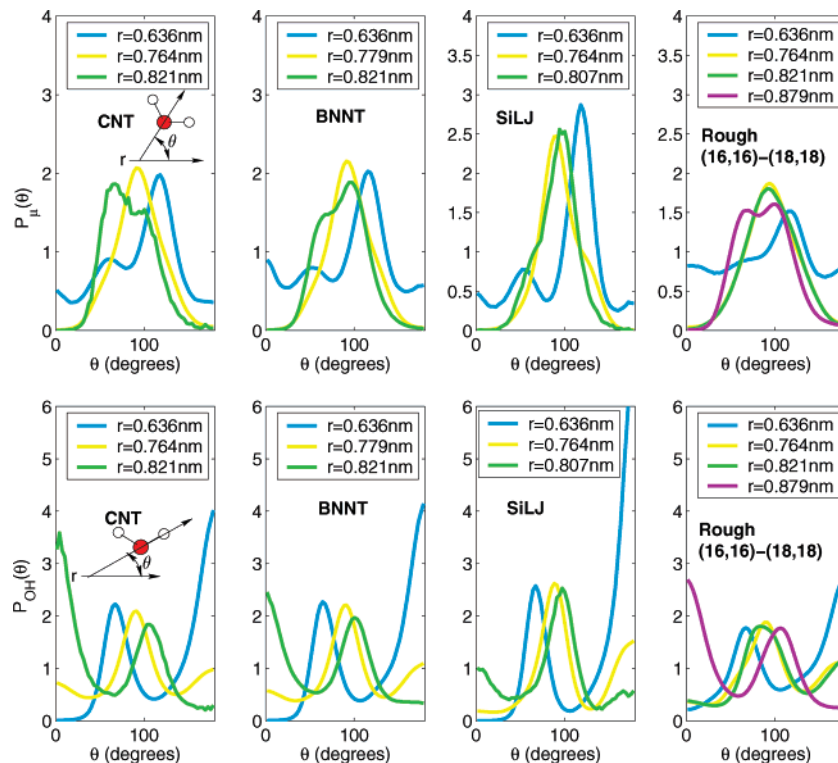


Figure 4. Dipole orientations (top) and OH bond orientations (bottom row) at various radial locations that represent, in the increasing order of r , (i) the valley of the water concentrations between the second and the first peak, (ii) the first water peak, and (iii) the depletion region. Note that for the CNT, the OH bond orientation is such that there is a “free” OH bond pointing to the wall.

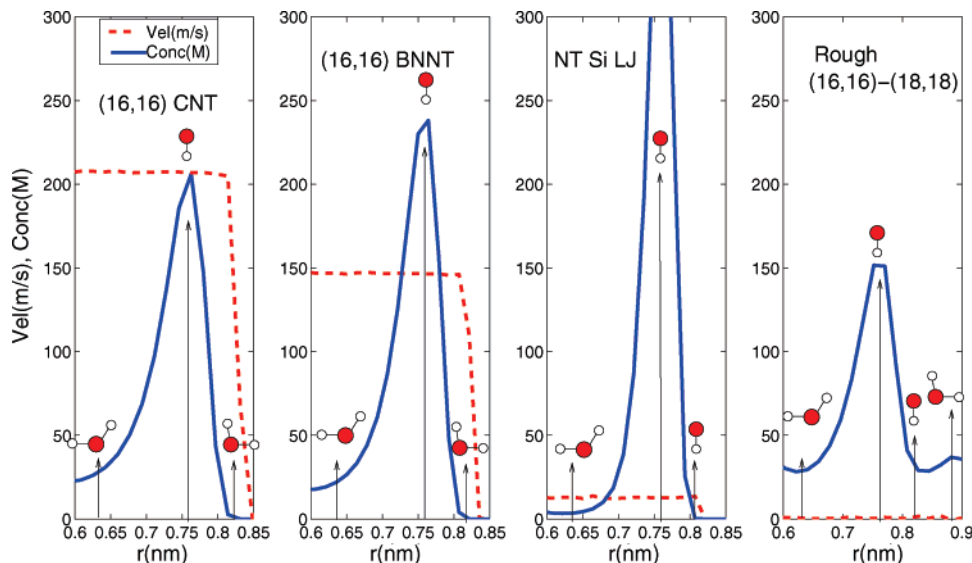


Figure 5. Schematic of water dipole orientations near the wall along with the concentrations. The velocity profiles are also shown to indicate the position of the depletion region and the water molecules in those regions. Water molecule in the depletion region of the CNT has a “free” OH bond, which is not found in NT with Si LJ.

orienting normal to the wall forming a planar layer even in the depletion region. There is no substantial number of “free” OH bonds or “dangling” OH bonds as compared to the CNT. The orientations are similar to the CNT for the first water peak and the valley of the first peak except that the distributions are more sharply defined due to the sharper layering of water in the NT with Si LJ. The water orientations in the BNNT lie in between that of the orientations for the CNT and the NT with Si LJ. In the rough tube, there is

practically no difference between the orientations at $r = 0.821$ nm and $r = 0.764$ nm, the location of the first water peak. The orientations in the cavity region at $r = 0.879$ seem to be almost at mirror image of that at the valley of the first water peak ($r = 0.636$ nm) showing a tightly integrated network of water molecules.

Because the water molecules in the depletion region for CNT have much more “free” OH bonds than the NT with Si LJ, we would expect the hydrogen bonding in the

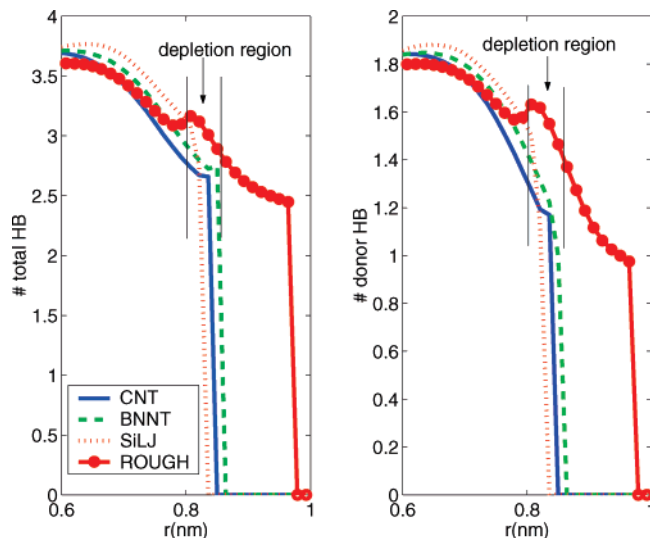


Figure 6. Total number of hydrogen bonds (left) and contribution of the donors (right) for different nanotubes. Because of the “free” OH bonds in the depletion region, the CNT has less number of hydrogen bonds as compared to the NT with Si LJ.

depletion region to be different for both cases. We investigated the average number of hydrogen bonds per water molecule as a function of the radial distance. A geometric definition of the hydrogen bond was used such that two water molecules are hydrogen-bonded if $r_{O-O} < 0.35$ nm and $\angle O...O-H < 30^\circ$. Figure 6 (left) shows the distributions of the hydrogen bonds per water molecule in the interfacial region for the water molecules. In the center of the tube, the number of H bonds is 3.7, the same as that in the bulk. In the depletion region, the number of hydrogen bonds follows the order $CNT < BNNT < NT \text{ with Si LJ} < \text{rough NT}$. Figure 6 (right) shows the hydrogen bonds from the donor hydrogens per water. In the depletion region, for CNT the number of donor hydrogen bonds is 1.17, and for NT with Si LJ the number of donor hydrogen bonds is 1.5. The “free” OH bonds in the depletion region do not contribute to the hydrogen bonding in the CNT. This is consistent with the experimental finding that hydrogen bonding between adjacent water molecules at hydrophobic interfaces is weak due to the presence of “free” OH bonds.²⁹ The number of hydrogen bonds we obtained in the interfacial region for the (16,16) CNT is very similar to that reported previously for water inside a (12,12) CNT⁷ and water outside a (16,0) CNT.⁸ The phenomena of velocity “jump” in cases with layered water concentrations that approach bulk values in the center, as in (16,16) tubes, are governed by the water structure in the depletion region. But as the tube diameter decreases and water approaches a single file profile, the water orientations and hydrogen bonding are radically different from that shown here. In a smaller diameter (6,6) tube with a single file water, the average number of hydrogen bonds is less than 2 because each water molecule can make an H bond only with the water molecules in front of it or behind it.^{6,7,9} In such cases, the flow rates could be influenced by factors other than that discussed here and is a topic of further study.

Another important point to note is that the flow rates are highly sensitive to the interatomic distances. The simulations

of BNNT presented here had a B–N bond length of 0.144 nm, which is slightly more than 0.142 nm (the bond length for CNT). For a BNNT tube with a bond length of 0.142 nm, the same as C–C bond length, the water velocity obtained was 42% higher than shown in Figure 1. Even a small increase in the bond length can make the region in the center of the hexagonal ring more attractive to LJ interactions that increase the oxygen concentrations and decreases the velocity “jump”.

To summarize, we have shown that the water structure such as the OH bond orientations and the hydrogen bonding in the depletion region where the water concentration is less than 5% of the bulk value has a direct effect on the enhancement of flow rates. A unique combination of features such as hexagonal structure, interatomic distances of 0.142 nm, and water orientations with “free” OH bonds pointing to the wall and the decreased hydrogen bonding in the depletion region contribute to large flow rates in CNTs in contrast to other materials such as polymer membranes with significant wall roughness.

Acknowledgment. This work was supported by NSF under Grants 0120978 (the Water CAMPWS Center at UIUC), 0325344, 0328162 (the nano-CEMMS Center at UIUC), 0523435, and by NIH under Grant PHS 2 PN2 EY016570B.

References

- (1) Majumder, M.; Chopra, N.; Andrews, R.; Hinds, B. *Nature* **2005**, *438*, 44.
- (2) Holt, J. K.; Park, H. G.; Wang, Y.; Stadermann, M.; Artyukhin, A. B.; Grigoropoulos, C. P.; Noy, A.; Bakajin, O. *Science* **2006**, *312*, 1034–1037.
- (3) Skoulidas, A. I.; Ackerman, D. M.; Johnson, J. K.; Sholl, D. S. *Phys. Rev. Lett.* **2002**, *89*, 185901.
- (4) Sokhan, V. P.; Nicholson, D.; Quirke, N. *J. Chem. Phys.* **2002**, *117*, 8531–8539.
- (5) Whitby, M.; Quirke, N. *Nat. Nanotechnol.* **2007**, *2*, 87–94.
- (6) Hummer, G.; Rasaiah, J.; Noworyta, J. *Nature* **2001**, *414*, 188–190.
- (7) Gordillo, M. C.; Marti, J. *Chem. Phys. Lett.* **2000**, *329*, 341–345.
- (8) Walther, J.; Jaffe, R.; Halicioglu, T.; Koumoutsakos, P. *J. Phys. Chem. B* **2001**, *105*, 9980–9987.
- (9) Mashl, R. J.; Joseph, S.; Aluru, N. R.; Jakobsson, E. *Nano Lett.* **2003**, *3*, 589–592.
- (10) Kalra, A.; Garde, S.; Hummer, G. *Proc. Natl. Acad. Sci. U.S.A.* **2003**, *100*, 10175–10180.
- (11) Zhu, F.; Schulten, K. *Biophys. J.* **2003**, *85*, 236–244.
- (12) Kolesnikov, A. I.; Zanotti, J.-M.; Loong, C.-K.; Thiyagarajan, P.; Moravsky, A. P.; Loutfy, R. O.; Burnham, C. J. *Phys. Rev. Lett.* **2004**, *93*, 035503.
- (13) Striolo, A. *Nano Lett.* **2006**, *6*, 633–639.
- (14) Kotsalis, E. M.; Walther, J. H.; Koumoutsakos, P. *Int. J. Multiphase Flow* **2004**, *30*, 995–1010.
- (15) Hanasaki, I.; Nakatani, A. *J. Chem. Phys.* **2006**, *124*, 144708.
- (16) Poynor, A.; Hong, L.; Robinson, I. K.; Granick, S.; Zhang, Z.; Fenter, P. A. *Phys. Rev. Lett.* **2006**, *97*, 266101.
- (17) Zhu, Y.; Granick, S. *Phys. Rev. Lett.* **2002**, *88*, 106102.
- (18) Won, C. Y.; Joseph, S.; Aluru, N. R. *J. Chem. Phys.* **2006**, *125*, 114701.
- (19) Won, C. Y.; Aluru, N. R. *J. Am. Chem. Soc.* **2007**, *129*, 2748–2749.
- (20) Lindahl, E.; Hess, B.; van der Spoel, D. *J. Mol. Model.* **2001**, *7*, 306–317.
- (21) Jakobtorweihen, S.; Verbeek, M. G.; Lowe, C. P.; Keil, F. J.; Smit, B. *Phys. Rev. Lett.* **2005**, *95*, 044501.
- (22) Chen, H.; Johnson, J.; Sholl, D. *J. Phys. Chem. B* **2006**, *110*, 1971–1975.
- (23) Berendsen, H. J. C.; Grigera, J. R.; Straatsma, T. P. *J. Phys. Chem.* **1987**, *91*, 6269–6271.

- (24) Nose, S. *Mol. Phys.* **2002**, *100*, 191–198.
(25) Hoover, W. G. *Phys. Rev. A* **1985**, *31*, 1695–1697.
(26) Parrinello, M.; Rahman, A. *J. Appl. Phys.* **1981**, *52*, 7182–7190.
(27) Koplik, J.; Banavar, J. R.; Willemsen, J. F. *Phys. Rev. Lett.* **1988**, *60*, 1282–1285.
(28) Liu, W.-T.; Zhang, L.; Shen, Y. R. *J. Chem. Phys.* **2006**, *125*, 144711.
(29) Scatena, L. F.; Brown, M. G.; Richmond, G. L. *Science* **2001**, *292*, 908–912.

NL072385Q